A LETTERS JOURNAL EXPLORING THE FRONTIERS OF PHYSICS

OFFPRINT

Correlated rearrangements of disordered colloidal suspensions in the vicinity of the reentrant glass transition

ZACHERY BROWN, MARTIN J. IWANICKI, MATTHEW D. GRATALE, XIAOGUANG MA, A. G. YODH and PIOTR HABDAS

EPL, **115** (2016) 68003

Please visit the website
www.epljournal.org

OVER
568,000
full text downloads in 2015

18 DAYS
average accept to online publication in 2015

20,300
citations in 2015

"We greatly appreciate the efficient, professional and rapid processing of our paper by your team."

Cong Lin
Shanghai University

Six good reasons to publish with EPL

We want to work with you to gain recognition for your research through worldwide visibility and high citations. As an EPL author, you will benefit from:

1. **Quality** – The 60+ Co-editors, who are experts in their field, oversee the entire peer-review process, from selection of the referees to making all final acceptance decisions.
2. **Convenience** – Easy to access compilations of recent articles in specific narrow fields available on the website.
3. **Speed of processing** – We aim to provide you with a quick and efficient service; the median time from submission to online publication is under 100 days.
4. **High visibility** – Strong promotion and visibility through material available at over 300 events annually, distributed via e-mail, and targeted mailshot newsletters.
5. **International reach** – Over 3200 institutions have access to EPL, enabling your work to be read by your peers in 100 countries.
6. **Open access** – Articles are offered open access for a one-off author payment; green open access on all others with a 12-month embargo.

Details on preparing, submitting and tracking the progress of your manuscript from submission to acceptance are available on the EPL submission website **epletters.net**.

If you would like further information about our author service or EPL in general, please visit **epljournal.org** or e-mail us at **info@epljournal.org**.

EPL is published in partnership with:

European Physical Society | Società Italiana di Fisica | EDP Sciences | IOP Publishing

A Letters Journal Exploring the Frontiers of Physics

September 2016

EPL, **115** (2016) 68003 www.epljournal.org
doi: 10.1209/0295-5075/115/68003

Correlated rearrangements of disordered colloidal suspensions in the vicinity of the reentrant glass transition

Zachery Brown[1], Martin J. Iwanicki[1(a)], Matthew D. Gratale[2], Xiaoguang Ma[2], A. G. Yodh[2] and Piotr Habdas[1(b)]

[1] *Department of Physics, Saint Joseph's University - Philadelphia, PA 19131, USA*
[2] *Department of Physics and Astronomy, University of Pennsylvania - Philadelphia, PA 19104, USA*

received 5 August 2016; accepted in final form 17 October 2016
published online 7 November 2016

PACS 82.70.Dd – Colloids
PACS 64.70.P- – Glass transitions of specific systems
PACS 05.40.Jc – Brownian motion

Abstract – We experimentally investigate correlated rearrangements (dynamic heterogeneity) in disordered colloidal suspensions as a function of increasing inter-particle attraction strength across the reentrant glass transition. Attractive interactions between constituent spheres are induced by polymer depletion forces at fixed particle volume fraction. We vary sample inter-particle attraction strength and concurrently measure particle trajectories by confocal microscopy at each attraction strength. The reentrant transition from repulsive glass to ergodic fluid and from ergodic fluid to attractive glass is readily observed. As the inter-particle attraction increases, we find that inter-particle bonding causes an increasing number of particles to undergo cooperative or correlated displacements; the length scale associated with these correlated rearrangements exhibits reentrant behavior. Other dynamical quantities such as the mean square displacement, the long-time diffusion constant, and the non-Gaussian parameter also exhibit changes as a function of attraction strength. Notably, the arrested (glass) states show small particle displacements at long lag times, whereas the fluid states exhibit fast dynamics over large length scales.

Introduction. – Suspensions of spherical colloidal particles are well-known to undergo a glass transition as a function of volume fraction, ϕ [1–4]. In hard-sphere glasses, for example, when ϕ is increased to a critical volume fraction, $\phi_g \approx 0.58$, long-range particle motion ceases and the system enters a nonequilibrium glassy state wherein configurational cages form around the particles and restrict their motion [1,2,5,6]. Interestingly, the introduction of short-range attractive interactions between particles in colloidal glasses can produce different classes of arrested states [7–9]. When the attraction strength between colloidal particles is increased from low to moderate, repulsive, hard-sphere like glasses "melt" into an ergodic fluid state [8–14], and as the attraction is increased further, the fluid system evolves into an attractive glass wherein bonding becomes the primary mechanism for arresting particle motion [8,9,13].

This so-called reentrant glass transition is accompanied by significant changes in particle dynamics, and many of these remarkable effects were revealed in light scattering [8,9,15], optical microscopy [11,12,14], simulation [13,16–18], and theoretical work [7,10,19,20]. In hard-sphere glasses, ergodic fluids, and attractive glasses, for example, the particle dynamics change on different timescales. At short times, most particles in these systems undergo relatively small displacements. However, heterogeneous rearrangements within the system permit particles to become significantly more mobile at long times [12–14,21,22]. Previous experiments have clearly shown qualitative differences between heterogeneous dynamics in repulsive and attractive glass states at higher volume fractions [21]; notably, attractive glasses exhibit correlated dynamics involving larger numbers of particles compared to repulsive glasses. In total, this work suggests that many critical insights needed for microscopic understanding of reentrant glass phenomenology can be derived from careful investigation of cooperative

(a) Present address: Department of Physics and Astronomy, University of Pennsylvania - Philadelphia, PA 19104, USA.
(b) E-mail: phabdas@sju.edu

rearrangements, or dynamic heterogeneity, in the vicinity of reentrance.

In this letter, we experimentally investigate correlated rearrangements (dynamic heterogeneity) in disordered colloidal suspensions as a function of increasing strength of the inter-particle attraction across the reentrant glass transition. Attractive interactions between constituent spheres are induced by polymer depletion forces [23–28] at fixed particle volume fraction. We employ confocal microscopy to capture time lapse images of the samples and to obtain their particle trajectories. The trajectory information enables us to quantify heterogeneous dynamics in these arrested systems as a function of attraction strength. We find significant differences in the number of cooperatively rearranging particles, as well as in the length scales over which colloidal particles rearrange in the various states. Interestingly, the length scale associated with these correlated rearrangement regions exhibits reentrant behavior. Furthermore, dynamical quantities such as the mean square displacement, the long-time diffusion constant, and the non-Gaussian parameter vary as a function of attraction strength. The arrested (glass) states show small particle displacements at long lag times, whereas the fluid states exhibit fast dynamics over large length scales. The results are described and rationalized herein.

Experimental methods. – The particles in this study are sterically stabilized poly-(methylmethacrylate) (PMMA) spheres (radius $R = 1.1\,\mu$m) containing rhodamine dye. The polydispersity in particle size is ∼5%, which suppresses crystallization. The PMMA spheres are suspended in a mixture of cyclohexylbromide (CXB) and decalin (∼85% CXB, ∼15% decalin) which matches the density and index of refraction of the colloidal particles with the solvent. To screen Coulombic interactions between PMMA particles, 2 mM tetra-butyl-ammonium chloride is added to the suspension [14,29]. Depletion attraction between PMMA particles is controlled by the addition of linear polystyrene (PS) polymer ($M_w = 5800000$ Da, $r_g = 92$ nm).

To capture images of PMMA particles, we use an Olympus IX81 inverted microscope with FV1000 confocal scanning head, a HeNe laser, and a 60× oil objective (N.A. = 1.42). We collect a series of 2D images (140.8 by 140.8 μm) in the bulk of the sample (with image plane located at least 25 μm from the coverslip) every 2.18 s. Standard tracking techniques are used to determine particle trajectories [30].

Samples are prepared through centrifugation and dilution in microscopy chambers made from a coverslip glued to a bottomless vial using UV curable epoxy. In these chambers, after the initial solvent evaporation, the volume fraction and polymer concentration remain constant throughout the process of mixing, tumbling, aging, and data collection. To avoid centrifuging to the random loose packing (RLP) state instead of the desired random close packing (RCP) state [31], the process of obtaining specific volume fraction of the colloidal suspension is carried out in two steps. First, colloidal suspensions are centrifuged to a relatively high volume fractions of $\phi \sim 0.50$. Next, after mixing, colloidal suspensions are centrifuged again to RCP where the volume fraction is $\phi_{RCP} \approx 0.66$ due to the polydispersity in particle size [14,32]. Finally, the samples are diluted to $\phi \approx 0.59$ using a mixture of PS polymer in liquid that matches density and index of refraction of the PMMA particles. The error in the volume fraction is set by the error in the measurement of RCP. The concentration of PS polymer, c_p, is calculated using the volume accessible to the polymer, $V(1-\phi)$, where V is the sample volume. We vary c_p from 0 to 1.7 mg/ml. A metal stir bar is added to the samples to mix the PS polymer with the colloidal suspension. Additionally, the suspensions undergo tumbling for at least 24 hours to ensure homogenous mixing of PS polymer within the PMMA colloidal suspension [14]. Finally, the samples are placed on the microscopy stage and left to equilibrate for several hours before images are recorded [12,14,22].

Introducing the PS polymer increases the viscosity of the background solvent, which decreases the rate of diffusion of the colloidal particles. Therefore, in order to compare samples with different PS concentrations, the times are reported in Brownian time units. The true collection time, t, is scaled by the time it takes a single particle to diffuse its own radius at a specific polymer concentration $t_B = tD_0/R^2$, where R is the particle radius and D_0 is the bare diffusion constant in the dilute solvent-polymer solution used in the experiments [12,14]. The bare diffusion constants for samples in this study are (in order of increasing c_p) 0.083 ± 0.004, 0.066 ± 0.005, 0.062 ± 0.006, 0.046 ± 0.002, 0.042 ± 0.004, and $0.029 \pm 0.001\,\mu\mathrm{m\,m^2/s}$.

Ensemble averaged dynamics. – Figure 1 presents a state diagram for the experimental system in which the solid squares correspond to samples studied, starting with a repulsive glass ($c_p = 0$ mg/ml) and ending with an attractive glass ($c_p = 1.7$ mg/ml). The transition lines are set by the attraction range, $\Delta = 2r_g$. Using known dynamical arrest transition lines for $\Delta = 0.16R$ [24], $\Delta = 0.28R$ [33], and $\Delta = 0.48R$ [8], we determine the state transition lines for $\Delta = 0.17R$ in our system. Note that the location of the transition lines is approximate due to colloidal particle size polydispersity [34].

Changes in particle dynamics with inter-particle attraction strength are quantified by the second moment of the particle displacement distribution or mean square displacement (MSD). In fig. 2 we plot the ensemble-averaged mean square displacement (normalized by the particle radius squared) *vs.* the Brownian lag time. For the $c_p = 0$ mg/ml and $c_p = 0.2$ mg/ml samples, the MSD exhibits a plateau at early lag times ($\Delta t_B < 10$) during which the particles are effectively caged by their neighbors [6]. The plateaus for these samples fall in the range of 0.001–$0.002R^2$. The plateau regime is followed by an upturn in the MSD which is typically attributed to cage rearrangements [12,14].

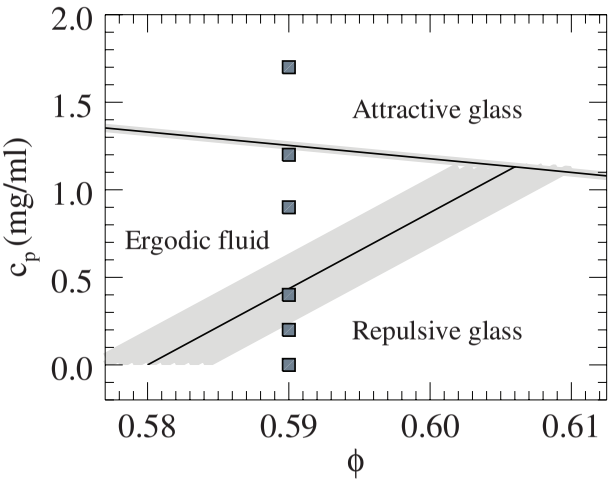

Fig. 1: The state diagram for the reentrant glass transition. Black squares denote the sample conditions from which data presented in this study are derived. The polymer concentration, c_p, sets the attractive strength, U, and the polymer radius of gyration, r_g, sets the attraction range. Solid black lines indicate transition boundaries between the various states for our attraction range, $\Delta = 0.17R$; the boundaries are estimated using known transition lines from experiment [8,33] and theory [24] as in ref. [33].

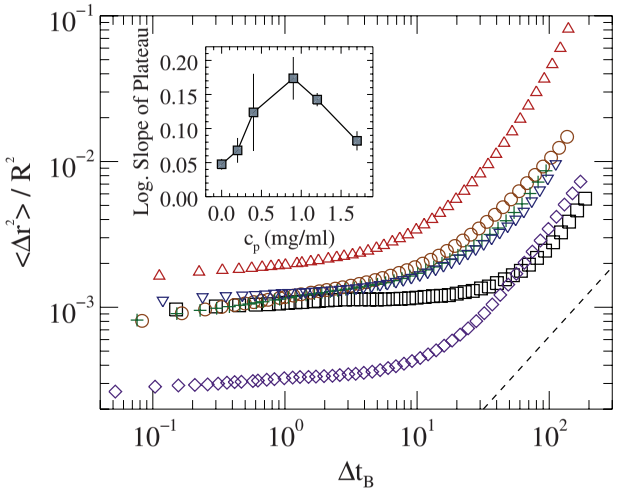

Fig. 2: (Color online) Mean square displacement (MSD) normalized by the colloidal particle radius squared plotted *vs.* Brownian lag time for $c_p = 0\,\mathrm{mg/ml}$ (□), $c_p = 0.2\,\mathrm{mg/ml}$ (▽), $c_p = 0.4\,\mathrm{mg/ml}$ (△), $c_p = 0.9\,\mathrm{mg/ml}$ (◯), $c_p = 1.2\,\mathrm{mg/ml}$(+), and $c_p = 1.7\,\mathrm{mg/ml}$ (◊). Dashed line has unit slope. Inset shows the logarithmic slope of the plateau of each MSD curve *vs.* c_p.

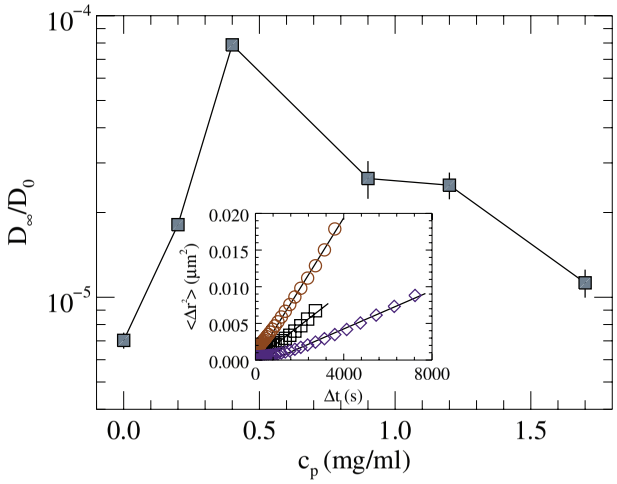

Fig. 3: (Color online) The long time diffusion constant, D_∞, normalized by the bare diffusion, D_0, constant plotted *vs.* polymer concentration c_p. The inset shows mean square displacements (MSDs) *vs.* Brownian lag time in samples with representative polymer concentrations, $c_p = 0\,\mathrm{mg/ml}$ (□), $c_p = 0.9\,\mathrm{mg/ml}$ (◯), and $c_p = 1.7\,\mathrm{mg/ml}$ (◊). The solid lines are best linear fits to the data at long times. The slopes of these lines are used to determine long time diffusion constants, D_∞.

The substantial increase in the value of the MSD for the $c_p = 0.4\,\mathrm{mg/ml}$ sample signifies melting of the hard-sphere like glass. The MSDs for $c_p = 0.9\,\mathrm{mg/ml}$ and $c_p = 1.2\,\mathrm{mg/ml}$ samples do not exhibit a plateau *i.e.*, the logarithmic slope determined from the MSD curves is the largest for 0.9 and 1.2 mg/ml samples, as shown in inset of fig. 2. Instead, we observe accelerated dynamics within these samples even at lag times during which the particles in the repulsive glass are confined to their cages. This effect provides evidence for an increase in local free volume, which permits particle cages to loosen and particles to move over larger length scales at intermediate Brownian lag times. These sample conditions, for which this change in dynamics with increased c_p is found, are consistent with the estimated transition boundary between the repulsive glass and ergodic fluid region shown in fig. 1. We note however, that samples with $c_p = 0.4\,\mathrm{mg/ml}$ and $c_p = 1.2\,\mathrm{mg/ml}$ are located close to a transition line and therefore may be classified either as a hard-sphere glass or an ergodic fluid, especially since the transition lines on the state diagram are expected to be broadened due to particle polydispersity.

The MSD arrest in attractive glasses is mainly due to bonding [8]. Indeed, the plateau of the MSD for the attractive glass sample ($c_p = 1.7\,\mathrm{mg/ml}$) observed in the present experiment is noticeably lower ($\sim 0.0002R^2$) than was observed for the repulsive glasses.

We extract the long-time diffusion constant, D_∞, by linearly fitting the MSD data at long Brownian lag times. Some of this data and corresponding linear fits are shown in the inset of fig. 3. Evidence of the reentrant glass transition is apparent in the plot of the long-time diffusion constant (D_∞) normalized by the bare diffusion constant, D_0, as a function of polymer concentration (fig. 3). D_∞/D_0 increases by roughly an order of magnitude when the system enters the ergodic fluid region, and then it decreases as the attractive glass region is approached. The initial increase for low to moderate attraction strengths reveals the melting of the glass and shows particles escaping

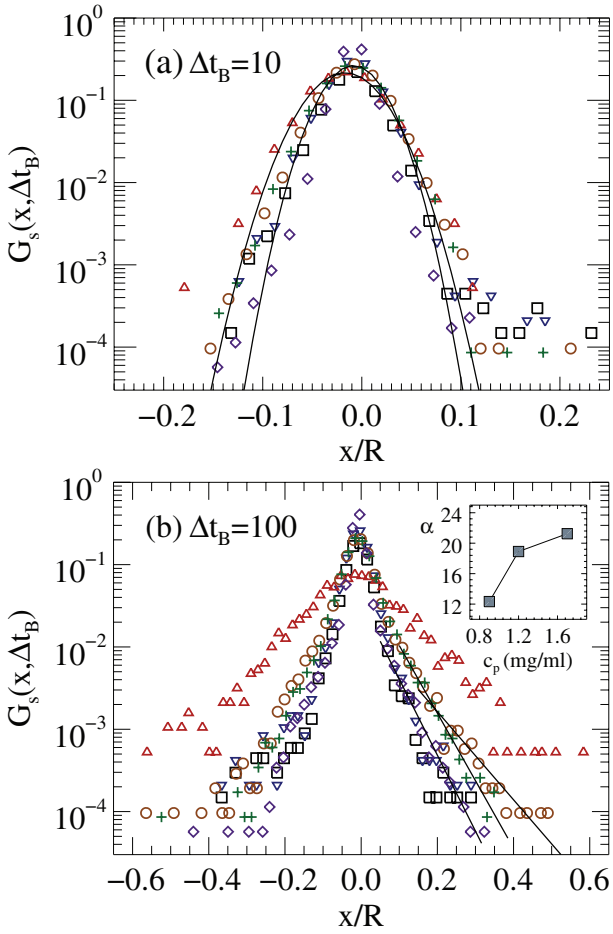

Fig. 4: (Color online) The "self"-parts of the van Hove correlation function, $G_s(x, \Delta t_B)$, for all samples. The correlation functions are plotted at lag times (a) $\Delta t_B = 10$ and (b) $\Delta t_B = 100$ Brownian units. $c_p = 0\,\mathrm{mg/ml}$ (□), $c_p = 0.2\,\mathrm{mg/ml}$ (▽), $c_p = 0.4\,\mathrm{mg/ml}$ (△), $c_p = 0.9\,\mathrm{mg/ml}$ (◯), $c_p = 1.2\,\mathrm{mg/ml}$ (+), and $c_p = 1.7\,\mathrm{mg/ml}$ (◊). Solid lines in (a) show representative Gaussian fits for $c_p = 0.4\,\mathrm{mg/ml}$ (△: wide fit) and $c_p = 0.9\,\mathrm{mg/ml}$ (◯: narrow fit). Solid lines in (b) show exponential fits to the tails of the $c_p = 0.9\,\mathrm{mg/ml}$ (◯), $c_p = 1.2\,\mathrm{mg/ml}$ (+), and $c_p = 1.7\,\mathrm{mg/ml}$ (◊) distributions. The inset in (b) shows the dimensionless decay rate of the correlation function exponential tails, α, *vs.* PS concentration. Larger α is indicative of smaller size correlated rearrangements.

from their cages; the ergodic fluids exhibit higher values of D_∞/D_0. The decrease of D_∞/D_0 when the systems enter the attractive glass state signifies a slowing of the particle dynamics, but in this case the decrease of the particle dynamics is due primarily to particle bonding rather than particle caging [12–14,21]; particle caging is the primary mechanism for attenuated dynamics in the repulsive glasses.

To further unravel the particle dynamics we calculate the "self"-portion of the van Hove distribution function $G_s(x, \Delta t_B) = \frac{1}{N}\sum_{i=1}^{N} \delta[x + x_i(0) - x_i(\Delta t_B)]$, where x_i is a particle displacement along one in-plane direction and N is the number of particles. The "self"-portion of the van Hove distribution function is essentially a probability distribution of displacements that describes the average motion of a particle after some lag time [33,35,36]. We plot G_s in one dimension for all samples at lag times of $\Delta t_B = 10$ (fig. 4(a)) and 100 (fig. 4(b)) in Brownian units.

For lag times of $\Delta t_B = 10$ (fig. 4(a)) the distributions are nearly Gaussian with small non-Gaussian tails. These tails correspond to a small number of particles undergoing correlated displacements. Indeed, at $\Delta t_B = 10$ the MSD for all samples, except the hard-sphere glass sample, starts exhibiting an upturn. The widths of these nearly Gaussian distributions scale with the value of the MSD at $\Delta t_B = 10$. The widest distribution corresponds to the $c_p = 0.4\,\mathrm{mg/ml}$ sample, where the value of the MSD is noticeably higher than the rest at $\Delta t_B = 10$. Furthermore, the narrowest distribution ($c_p = 1.7\,\mathrm{mg/ml}$) corresponds to the smallest value of the MSD at $\Delta t_B = 10$. The hard sphere ($c_p = 0\,\mathrm{mg/ml}$) sample shows a narrow distribution, but it is considerably wider than the attractive glass ($c_p = 1.7\,\mathrm{mg/ml}$). This observation reflects the tight bonding in the attractive glasses and the increased mobility at short times in ergodic fluids.

For $\Delta t_B = 100$ (fig. 4(b)), however, the distributions widen for all c_p's, indicating the presence of large particle displacements. This increase in particle mobility is accompanied by the increasingly non-Gaussian tails of the distributions. It has been suggested that the central portion of the van Hove distribution for some colloidal glass formers should take on a Gaussian shape [33,37]. Additionally, in systems of attractive colloids undergoing dynamical arrest, the tails appear to be well fit by exponentials [37]. Regardless, the existence of any non-Gaussian tails provides evidence of particles undergoing large displacement events and indicates that the samples are experiencing increasingly heterogeneous dynamics.

As the polymer concentration, c_p, increases, we observe significant changes in the peaks and tails of the distributions at $\Delta t_B = 100$. These changes provide further illustration of the reentrant glass transition. The hard-sphere like samples ($c_p = 0\,\mathrm{mg/ml}$ (□) and $c_p = 0.2\,\mathrm{mg/ml}$ (▽)) show well defined Gaussian peaks for displacements ranging from 0 to $\sim 0.1R$, with relatively small tails that do not fit to an exponential function very well. It seems that at low attraction strengths exponential tails are not present.

The $c_p = 0.4\,\mathrm{mg/ml}$ sample (△) shows the widest distribution width, but the tails still do not exhibit an exponential behavior. The change from hard-sphere to moderate attraction strengths is accompanied by a melting of the glass. This transition is seen in the widening of the van Hove distribution, which provides evidence that the particles have become increasingly mobile. By contrast, the distributions in the ergodic fluid region, for $c_p = 0.9\,\mathrm{mg/ml}$ (◯) and $c_p = 1.2\,\mathrm{mg/ml}$ (+), exhibit large exponential tails of mobile particles. Further, their Gaussian peaks narrow as c_p increases.

This latter trend continues into the attractive glass regime ($c_p = 1.7\,\mathrm{mg/ml}$ ◊), where the distribution shows

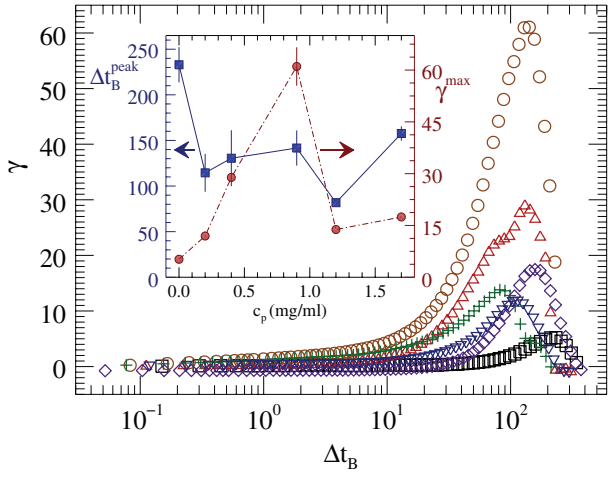

Fig. 5: (Color online) The non-Gaussian parameter, γ, *vs.* Brownian lag time, $c_p = 0\,\mathrm{mg/ml}$ (□), $c_p = 0.2\,\mathrm{mg/ml}$ (▽), $c_p = 0.4\,\mathrm{mg/ml}$ (△), $c_p = 0.9\,\mathrm{mg/ml}$ (◯), $c_p = 1.2\,\mathrm{mg/ml}$ (+), and $c_p = 1.7\,\mathrm{mg/ml}$ (◇). The inset shows the amplitude of the non-Gaussian peak, γ^{max} (●) and Brownian lag time at which the non-Gaussian parameter peaks, Δt_B^{peak} (■) *vs.* c_p.

a very narrow Gaussian peak corresponding to displacements of 0 to $\sim 0.05R$. This peak is narrower than those in the ergodic fluids, and its width is half that of the peak of the $c_p = 0\,\mathrm{mg/ml}$ hard-sphere glass sample. This decrease in the peak width from the ergodic fluid to the attractive glass region provides evidence of tightening inter-particle bonds. In transitioning from the liquid region into the attractive glass, the exponential tails of the distributions tend to decay faster with increasing attraction strength (inset in fig. 4(b)). The exponential tails of the distributions are due to particles that experience relatively large, correlated displacements and are of the form $G_s \sim \exp(-\frac{\alpha x}{R})$. Thus, the magnitude (in dimensionless units) of the tail's exponential decay rate, α, inversely characterizes the spatial extent of the dynamical heterogeneity. α becomes larger as c_p increases from 0.9 mg/ml to 1.7 mg/ml. This observation suggests that for relatively high attraction strengths corresponding to the attractive glass state, correlated motion is limited to a small range of displacements.

To characterize the particle displacement distributions and their deviations from Gaussian dynamics, we calculate the non-Gaussian parameter, $\gamma(\Delta t_B) = \frac{1}{1+2/d}\langle \Delta r^2 \rangle \langle \frac{1}{\Delta r^2} \rangle - 1$, where d is the sample dimension [38,39]. Larger values of γ are indicative of more correlated and non-Gaussian dynamics. In fig. 5 we show the non-Gaussian parameter *vs.* Brownian lag time Δt_B. All samples exhibit Gaussian behavior at short Brownian lag times where the value of their non-Gaussian parameters are small.

Notice however, all samples exhibit a clear peak in the non-Gaussian parameter at long Brownian lag times. For each of these curves we determine the maximum value of each peak, γ^{max}, and the Brownian lag time at which this maximum occurs, Δt_B^{peak}. In the inset of fig. 5 we plot both γ^{max} (●) and Δt_B^{peak} (■) *vs.* c_p. Notice that the amplitude of the non-Gaussian parameter is indicative of the reentrance behavior; γ^{max}, increases with c_p into the ergodic fluid region and then decreases as c_p is increased further. Specifically, γ^{max} is largest for the $c_p = 0.9\,\mathrm{mg/ml}$ sample, which exhibits the most non-Gaussian dynamics and largest particle displacements. The plot of Δt_B^{peak} *vs.* c_p suggests that non-Gaussian dynamics occur at the longest Brownian lag times in the arrested states, decreasing slightly in the ergodic fluids. Since non-Gaussian dynamics are associated with correlated rearrangements, the fact that the non-Gaussian parameter is peaked at the longest times is indicative of the fact that caging (repulsive glasses) or bonding (attractive glass) is more permanent in the arrested glass states (*e.g.*, compared to the fluid state).

Dynamical heterogeneity. – The non-Gaussian parameter is calculated by averaging over all displacements for a given lag time. Thus, the non-Gaussian parameter is limited; it is unable, for example, to evaluate how the dynamics associated with cage escapes, inter-particle bond breaking, and cluster rearrangements vary over the full range of particle displacements. To ameliorate this weakness in our analysis, we compute the self-overlap function, $Q_2(a, \Delta t_B) = \frac{1}{N}\sum_{i=1}^{N} \exp(-\frac{\Delta r_i^2}{2a^2})$, which measures how much particles have moved relative to a probe length a. For each sample, Q_2 is calculated across a range of relevant lengths, a, and across a range of Brownian lag times. Then, for each a and Δt_B, the four-point susceptibility, $\chi_4 = N(\langle Q_2(a, \Delta t_B)^2 \rangle - \langle Q_2(a, \Delta t_B) \rangle^2)$, is also computed. The quantity χ_4 is the variance of the statistical fluctuations of Q_2; it measures the spatio-temporal rearrangement heterogeneity within the samples. Larger values of χ_4 represent more heterogeneous dynamics, and the magnitude of χ_4 scales with the number of particles involved in correlated motion at particular length (a) and time (Δt_B) scales [6,21,40]. Here we study the four-point susceptibility as a function of both probing length scale, a, and time scale, Δt_B.

Importantly, we find significant differences in χ_4 as a function of increased inter-particle attraction strength. In fig. 6 we plot contour plots of χ_4 as a function of both probe length a and Brownian lag time Δt_B for each sample. In all cases χ_4 peaks at a specific a^{max} and Δt_B^{max}. The magnitude of this peak rises steadily with c_p, as seen in the contour plots (fig. 6), and in the plot of the peak value, χ_4^{max}, *vs.* c_p (fig. 7(a)). The observations suggest that as inter-particle attraction increases, so does the number of particles undergoing heterogeneous rearrangements. Notice also that the number of particles participating in correlated rearrangements in the attractive glass is $\sim$7 times larger than in the hard-sphere glass (fig. 7(a)). A previous study of a different colloidal system came to similar conclusions regarding correlated rearrangements in attractive *vs.* repulsive glassy systems [21].

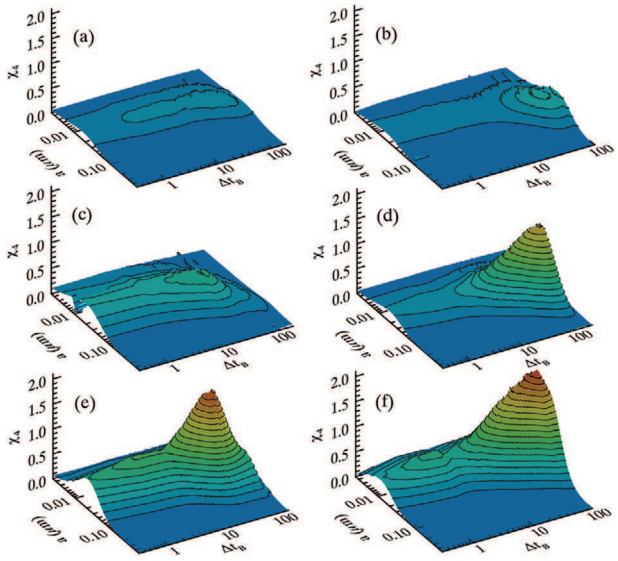

Fig. 6: (Color online) χ_4 as a function of probe length, a, and lag time, Δt_B, for (a) $c_p = 0.0\,\mathrm{mg/ml}$, (b) $c_p = 0.2\,\mathrm{mg/ml}$, (c) $c_p = 0.4\,\mathrm{mg/ml}$, (d) $c_p = 0.9\,\mathrm{mg/ml}$, (e) $c_p = 1.2\,\mathrm{mg/ml}$, and (f) $c_p = 1.7\,\mathrm{mg/ml}$. Each color level represents an interval of 0.1 in χ_4.

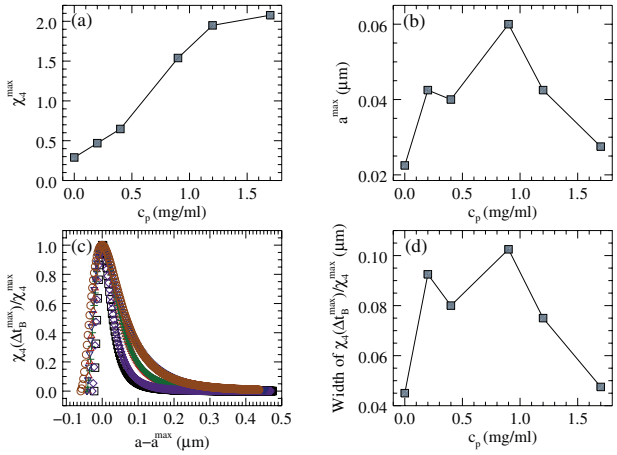

Fig. 7: (Color online) (a) The maximum value of χ_4 as a function of polymer concentration. (b) The probe length corresponding to χ_4^{max}, a^{max}, as a function of polymer concentration. (c) A plot of χ_4 normalized by χ_4^{max} at Δt_B^{max} as a function of $a-a^{max}$ for $c_p = 0\,\mathrm{mg/ml}$ (□), $c_p = 0.2\,\mathrm{mg/ml}$ (▽), $c_p = 0.4\,\mathrm{mg/ml}$ (△), $c_p = 0.9\,\mathrm{mg/ml}$ (◯), $c_p = 1.2\,\mathrm{mg/ml}$ (+), and $c_p = 1.7\,\mathrm{mg/ml}$ (◊). (d) Full width at half-maximum of χ_4/χ_4^{max} *vs.* c_p.

In the present study, we find that the probe length corresponding to the largest dynamical heterogeneity, a^{max}, again follows the reentrant glass transition behavior. It initially increases as a function of polymer concentration (fig. 7(b)). Then, as the attractive glass is approached, inter-particle bonding increasingly becomes the driving mechanism for the arrest, and a^{max} decreases to a similar value as that for the hard-sphere glass. We expect that a^{max} would decrease to an even lower value at further increased polymer concentrations (increased inter-particle attraction). This finding demonstrates that correlated particle motion in the repulsive and attractive glasses occurs over shorter length scales than found in the ergodic fluid region. The finding is in excellent agreement with simulation studies [13], which suggested that cages become looser as the ergodic fluid region is entered, and thus the heterogeneous dynamics associated with rearrangements occur over larger length scales. On the other hand, the Brownian lag time, Δt_B^{max}, that corresponds to the maximum of χ_4, varies little as a function of c_p and does not exhibit any clear trend.

To find the range of probe lengths over which dynamics are most heterogeneous, we plot χ_4 normalized by χ_4^{max} at Δt_B^{max} as a function of $a - a^{max}$ for each c_p (fig. 7(c)). Then, we determine its full width at half-maximum, *e.g.*, the full width at half-maximum of the χ_4/χ_4^{max} curve, and we plot this width *vs.* c_p (fig. 7(d)). Interestingly, we find that width of χ_4/χ_4^{max} exhibits a similar reentrance behavior as a^{max}. Evidently, the heterogeneous dynamics in arrested states occur over a much more narrow range of length scales compared to ergodic fluids. Alternatively, the particle rearrangements in the ergodic fluids are spread over a wide range of lengths (*e.g.*, wider than in the arrested states).

Lastly we note that both the length scale that maximizes χ_4, a^{max}, and the full width at half-maximum of χ_4/χ_4^{max}, have similar values in the repulsive and attractive glasses (fig. 7(b) and (d)). This observation may be interpreted as due to the fact that in attractive glasses, bonding and cages are both important, and the caging length scale is intrinsically preserved in the system even as the inter-particle attraction strength is increased. Indeed, computer simulations on timescales much longer than available experimentally have revealed that arrest in attractive glasses is topological and is not only due to bonding, but to caging as well [13].

Conclusions. – Confocal microscopy images of dense colloidal suspensions at a fixed volume fraction were collected as the inter-particle attraction strength was systematically increased. Within the ranges of operation, $\phi = 0.59$ and $c_p = 0$–$1.7\,\mathrm{mg/ml}$, three characteristic sample states were observed. At the lowest PS concentrations and therefore the lowest inter-particle attraction strengths, the repulsive glasses showed evidence of relatively small correlated rearrangements over small distances, corresponding to cage rearrangements and cage escapes. At larger attraction, ergodic fluids exhibited accelerated dynamics at short times and increasingly heterogeneous dynamics over the largest length scales. Rearrangements within these samples were larger than in the repulsive glass, and heterogeneous dynamics were found across large length scales. Finally, an attractive glass was observed showing the effects of strong particle bonding and exhibiting large numbers of rearranging particles; it was

qualitatively different than the repulsive glass. In a previous experiment [21], the dynamics of repulsive glasses and strongly attractive glasses were studied and characterized. The present work, by contrast, has pushed significantly beyond the previous investigation. It has employed several additional theoretical tools and, importantly, includes an analysis of repulsive glasses, ergodic fluids, and attractive glasses that permit improved characterization of the reentrant glass transition.

Future experimental studies of the reentrant glass transition would benefit from full 3-dimensional spatial scans of the samples. Particles could then be reliably tracked for longer times as they also move in the direction perpendicular to the optical image plane. Additionally, rearrangement regions could be characterized by their shape and size, thereby providing information that could be used to further distinguish between the three states of the reentrant glass transition.

* * *

We thank Kevin B. Aptowicz, Zoey S. Davidson, Tim Still, and Wei-Shao Wei for helpful discussions. We thank Andrew B. Schofield for supplying colloidal particles. ZB, MJI, and PH gratefully acknowledge financial support from the National Science Foundation through Grant No. RUI-1306990. MDG, XM, and AGY gratefully acknowledge financial support from the National Science Foundation through Grant No. DMR12-05463, the Penn MRSEC Grant No. DMR11-20901 and its optical microscopy SEF, and NASA Grant No. NNX08AO0G.

REFERENCES

[1] Pusey P. N. and van Megen W., *Nature (London)*, **320** (1986) 340.
[2] Pusey P. N. and van Megen W., *Phys. Rev. Lett.*, **59** (1987) 2083.
[3] van Megen W. and Underwood S. M., *Phys. Rev. Lett.*, **70** (1993) 2766.
[4] Bryant G., Williams S. R., Qian L., Snook I. K., Perez E. and Pincet F., *Phys. Rev. E*, **66** (2002) 060501.
[5] Weeks E. R. and Weitz D. A., *Phys. Rev. Lett.*, **89** (2002) 95704.
[6] Narumi T., Franklin S. V., Desmond K. W., Tokuyama M., Weeks E. R., *Soft Matter*, **7** (2011) 1472.
[7] Dawson K. A., Foffi G., Fuchs M., Götze W., Sciortino F., Sperl M., Tartaglia P., Voigtmann T. and Zaccarelli E., *Phys. Rev. E*, **63** (2000) 11401.
[8] Pham K. N., Puertas A. M., Bergenholtz J., Egelhaaf S. U., Moussaid A., Pusey P. N., Schofield A. B., Cates M. E., Fuchs M. and Poon W. C. K., *Science*, **296** (2002) 104.
[9] Eckert T. and Bartsch E., *Phys. Rev. Lett.*, **89** (2002) 125701.
[10] Poon W. C. K., *MRS Bull.*, **29** (2004) 96.
[11] Simeonova N. B., Dullens R. P. A., Aarts D. G. A. L., de Villeneuve V. W. A., Lekkerkerker H. N. W. and Kegel W. K., *Phys. Rev. E*, **73** (2006) 041401.
[12] Kaufman L. J. and Weitz D. A., *J. Chem. Phys.*, **125** (2006) 074716.
[13] Zaccarelli E. and Poon W. C. K., *Proc. Natl. Acad. Sci. U.S.A.*, **106** (2009) 1.
[14] Latka A., Han Y., Alsayed A. M., Schofield A. B., Yodh A. G. and Habdas P., *EPL*, **86** (2009) 58001.
[15] Pham K. N., Egelhaaf S. U., Pusey P. N. and Poon W. C. K., *Phys. Rev. E*, **69** (2004) 11503.
[16] Puertas A. M., Fuchs M. and Cates M. E., *Phys. Rev. Lett.*, **88** (2002) 98301.
[17] Puertas A. M., Fuchs M. and Cates M. E., *J. Chem. Phys.*, **121** (2004) 2813.
[18] Pusey P. N., Zaccarelli E., Valeriani C. and Sanz E., *Philos. Trans. R. Soc. A*, **367** (2009) 4993.
[19] Bergenholtz J. and Fuchs M., *Phys. Rev. E*, **59** (1999) 5706.
[20] Dawson K. A., *Curr. Opin. Colloid Interface Sci.*, **7** (2002) 218.
[21] Zhang Z., Yunker P., Habdas P. and Yodh A. G., *Phys. Rev. Lett.*, **107** (2011) 208303.
[22] van de Laar T., Higler R., Schröen K. and Sprakel J., *Sci. Rep.*, **6** (2016) 22725.
[23] Asakura S. and Oosawa F., *J. Chem. Phys.*, **22** (1954) 1255.
[24] Illet S. M., Orrock A., Poon W. C. K. and Pusey P. N., *Phys. Rev. E*, **51** (1995) 1344.
[25] Verma R., Crocker J. C., Lubensky T. C. and Yodh A. G., *Macromolecules*, **33** (2000) 177.
[26] Starrs L., Poon W. C. K., Hibberd D. J. and Robins M. M., *J. Phys.: Condens. Matter*, **14** (2002) 2485.
[27] Poon W. C. K., *J. Phys.: Condens. Matter*, **14** (2002) R859.
[28] Foffi G., De Michele C., Sciortino F. and Tartaglia P., *Phys. Rev. Lett.*, **94** (2005) 078301.
[29] Yethiraj A. and van Blaaderen A., *Nature*, **421** (2003) 513.
[30] Crocker J. C. and Grier D. G., *J. Colloid Interface Sci.*, **179** (1996) 298.
[31] Liber S. R., Borovich S., Butenko A., Schofield A. B. and Sloutskin E., *Proc. Natl. Acad. Sci. U.S.A.*, **110** (2013) 5769.
[32] Schaertl W. and Sillescu H., *J. Stat. Phys.*, **77** (1994) 1007.
[33] Gao Y. and Kilfoil M. L., *Phys. Rev. Lett.*, **99** (2007) 078301.
[34] Zaccarelli E., *Phys. Complex Colloids*, **19** (2013) 95.
[35] Rahman A., *Phys. Rev.*, **136** (1964) A405.
[36] Hopkins P., Fortini A., Archer A. J. and Schmidt M., *J. Chem. Phys.*, **133** (2010) 224505.
[37] Chaudhuri P., Gao Y., Berthier L., Kilfoil M. and Kob W., *J. Phys.: Condens. Matter*, **20** (2008) 244126.
[38] Flenner E. and Szamel G., *Phys. Rev. E*, **72** (2005) 011205.
[39] Saltzman E. and Schweizer K., *Phys. Rev. E*, **74** (2006) 061501.
[40] Brambilla G., El Masri D., Pierno M., Berthier L., Cipelletti L., Petekidis G. and Schofield A. B., *Phys. Rev. Lett.*, **102** (2009) 085703.